Optimisation of unsteady flight in learned avian perching manoeuvres

Marco Klein Heerenbrink[1*], Lydia A. France[1,2*], Graham K. Taylor[1]

1. Department of Zoology, University of Oxford, OX1 3SZ, UK
2. Current address: The Alan Turing Institute, London, NW1 2DB, UK

* These authors contributed equally to this work.

Flight is the most energetically costly activity that animals perform, making its optimisation crucial to evolutionary fitness. Steady flight behaviours like migration and commuting are adapted to minimise cost-of-transport or time-of-flight[1], but the optimisation of unsteady flight behaviours is largely unexplored[2,3]. Unsteady manoeuvres are important in attack, evasion, and display, and ubiquitous during take-off and landing. Whereas smaller birds may touchdown slowly by flapping[2,4-8], larger birds swoop upward to perch[9,10] – presumably because adverse scaling of their power margin prohibits slow flapping flight[11], and because swooping transfers excess kinetic to potential energy[9,10,12]. Landing is especially risky in larger birds[7,13] and entails reaching the perch with appropriate velocity and pose[14-17], but it is unknown how this challenging behaviour is optimised. Here we show that Harris' hawks *Parabuteo unicinctus* minimise neither time nor energy when swooping between perches for food, but instead minimise the gap they must close under hazardous post-stall conditions. By combining high-speed motion capture of 1,592 flights with dynamical modelling and numerical optimization, we found that the birds' choice of where to transition from powered dive to unpowered climb minimised the distance from the perch at which they stalled. Time and energy are therefore invested to maintain the control authority necessary to execute a safe landing, rather than being minimized continuously as they have been in applications of autonomous perching under nonlinear feedback control[15] and deep reinforcement

learning[18,19]. Naïve birds acquire this behaviour through end-to-end learning, so penalizing stall distance using machine learning may provide robustness in autonomous systems.

Perching is among the most challenging flight manoeuvres that birds perform[9,10], inspiring efforts to achieve similar capability in autonomous vehicles[12,15,16,18,20-24]. Perched landings are particularly demanding, because the lack of a runway to bleed speed after touchdown creates a precise targeting requirement that is compromised by the difficulty of maintaining control authority at the low airspeeds necessary before touchdown[12,15,20]. Although some kinetic energy may be converted to gravitational potential energy when climbing[9,10,12], most is lost through aerodynamic drag or else dissipated by the legs and perch[2,4,25-27]. Aerodynamic braking is therefore critical to avoiding a dangerously energetic collision, but the associated high angles of attack compromise lift production and hence flight control as the flow over the wing stalls[12,15,20,24]. The rapid pitch-up manoeuvre that birds execute when perching is expected to delay stall[7,9,10,22,24,28], transiently increasing lift and drag through rotational circulatory forces and added mass effects[29]. Even so, stall cannot be delayed indefinitely, and is desirable for braking at the end of the manoeuvre[12,15,18,20-24]. There must therefore come a point post-stall when the bird loses control authority and can only recover errors or disturbances by flapping. The extreme rapidity of the pitch-up manoeuvre makes forward-planning of its entry conditions critical[18], but begs the question of how the flight trajectory and control inputs are optimised. More generally, the pendulum-like dynamics of swooping provide a tractable test case for asking how animals optimise complex unsteady motions through end-to-end learning.

To address these questions, we rigged a large custom-built motion capture studio to record captive-bred Harris' hawks flying spontaneously between perches spaced 5, 7, 9, or 12 m apart at 1.25m height for food (see Methods; Supplementary Movie 1). The hawks wore

retroreflective markers enabling us to reconstruct their flight trajectories at 120 or 200 Hz (Fig. 1). Three of the $n = 4$ birds were juveniles that had only flown short hops previously; the other was an experienced adult. We collected trajectory data from 1,592 flights during 11 weeks of trials, following an initial fitness-training period at 12 m perch spacing (see Methods). The juvenile birds flew directly between the perches on their first few training flights (Fig. 2A), but soon adopted the swooping behaviour characteristic of experienced birds (Fig. 2B-E). Swooping was initiated by jumping forwards into a dive involving several powerful wingbeats, which transitioned into a climb involving a rapid pitch-up manoeuvre that ended with the body almost vertical and the wings outstretched as the feet contacted the perch (Fig. 1). Climbing comprised mainly gliding flight, with occasional half-flaps that we interpret as corrective control inputs, rather than as wingbeats supplying forward thrust. Trajectory geometry was well summarised by the location of its point of minimum height, where the transition from powered to unpowered flight occurred. The birds dived deeper at wider perch spacing, but the longitudinal position of the transition point was always similar relative to the perches, at 61.2 ± 2.84 % of the spacing distance (mean ± s.d.). The birds only dived to within one semispan (≤ 0.5 m) of the ground at 12 m perch spacing (Fig. 2E), so although ground effect may have briefly assisted flight in this case[30], its exploitation is unlikely to have motivated swooping in general.

The consistency with which different birds independently acquired the same characteristic swooping behaviour (Fig. 2) suggests that this is the result of individual reinforcement learning against some common optimisation criterion. Take-off and landing are energetically demanding flight behaviours because of the high aerodynamic power requirements of slow flight. Guided by previous work on perching parrotlets[2], we therefore hypothesised that our hawks learned trajectories minimising the energetic cost of flight between perches. An alternative hypothesis is that the hawks learned trajectories minimising

time of flight[1], which could make sense for a predator adapted to exploit fleeting feeding opportunities[3]. This would also have maximised the net rate of energy gain[1], because the energy gained through feeding greatly exceeded the energy expended to obtain it. Can either hypothesis explain the swooping that we observed? Diving uses gravitational acceleration to reach faster speeds quicker[31], which could reduce flight duration if the increased path length were outweighed by the gain in speed. This is analogous to the classical brachistochrone problem, in which a curved path minimises the travel time of a particle falling between two points under the influence gravity[32]. Flying faster also reduces the mechanical work required at speeds below the minimum power speed[31], so it seems intuitive that swooping could reduce both the time and energetic cost of flight.

We used a simulation model to assess how these two performance objectives were influenced by the choice of flight trajectory, comparing the optimal solutions to the trajectories observed at different perch spacings. We used a two-phase model comprising a powered dive switching to an unpowered climb at the point flight became level (see Methods). This captures the characteristic swooping behaviour of experienced birds and includes the direct flight behaviour of inexperienced birds as a limiting case. Our simulations incorporated individual variation in flight morphology and take-off speed (Table 1), and we assumed for simplicity that the aerodynamic lift and power were held constant on each flight phase. We calculated aerodynamic thrust as the ratio of power to speed, and modelled aerodynamic drag by parameterising a theoretical drag polar using published measurements from Harris' hawks[33]. With these assumptions, and for a given power setting, every modelled flight trajectory is parameterised by its initial flight path angle (γ_0) and lift setting (L_{dive}) on the dive phase. These two parameters jointly determine the entry conditions for the unpowered climb phase, defined by the position ($x_{\mathrm{T}}, y_{\mathrm{T}}$) and velocity ($V_{\mathrm{T}}, 0$) of the bird at the transition point. The lift setting for the unpowered climb phase (L_{climb}) is then uniquely determined by the constraint that the

trajectory must intercept the landing perch at a reasonable landing speed. By setting the terminal speed of the simulations to the mean contact speed for each bird (Table 1), we identified a line of feasible parameter settings that would bring the bird safely to the perch (Fig. 3). A maximum specific anaerobic power output of 50 W kg^{-1} was estimated previously[34] from Harris' hawks climbing with loads. However, it is unlikely our birds would have flown at full power when diving, so we estimated a specific power setting for each bird to best match the observed data across all distances (Fig. 3). Minimising the sum of the squared distance of the observed transition points to the line of feasible transition points predicted by the model yielded specific power estimates ranging from 18.7 to 22.9 W kg^{-1} (Table 1). This is less than the additional power that Harris' hawks use for climbing[34,35], suggesting that our birds used less than half their available power when diving.

The simulations reveal some unexpected results. First, although diving allows faster speeds to be reached quicker, it also reduces the powered fraction of the flight. Shortening the unpowered climb phase proves more effective in decreasing flight duration, and the time-optimal solution is therefore a shallow powered dive followed by a short unpowered climb (Fig. 3C). Second, although the lift-to-drag ratio is reduced at the higher speeds reached in a dive, this increased efficiency of lift production is outweighed by the increased lift required to turn into the climb. The energy-optimal solution is therefore an almost straight flight trajectory with a long, flat unpowered phase in which airspeed is lost to maintain altitude (Fig. 3A). Hence, neither time nor energy minimization can straightforwardly explain the deep swooping behaviour of experienced birds, which contrasts with most steady, and some unsteady, flight behaviours[1,2]. It is possible in principle that the hawks made a particular trade-off between time and energy leading to the selection of an intermediate transition point, but we think it more likely that they optimised a different performance objective entirely.

Minimizing either time or energy requires very high lift coefficients, $C_L = 2L/(\rho V^2 S)$, where L is lift, ρ is air density, V is airspeed, and S is wing area. In the time-optimal case, this arises because of the need to provide high lift for braking on a short unpowered climb (Fig. 3C). In the energy-optimal case, it arises because of the need to sustain weight support at ever-decreasing airspeed on a long unpowered phase (Fig. 3A). High lift coefficients can be achieved transiently during unsteady perching manoeuvres[36,37], with peak values up to $C_L \leq 5$ predicted in modelling of the rapid pitch-up manoeuvre[29]. Nevertheless, stall cannot be delayed indefinitely, and will compromise control authority on final approach[12,15,20,24]. This suggests a different performance objective relevant to unsteady flight behaviours: minimise the distance flown post-stall. We implemented this optimisation criterion by selecting the transition point that minimised the distance flown at $C_L > 4$, which accommodates the very high lift coefficients that can be achieved transiently during a rapid pitch-up manoeuvre, whilst nevertheless penalising deep stall. The predicted location of the optimal transition point was robust to this choice, moving $\leq 1.6\%$ of perch spacing distance per unit decrement in the threshold value of C_L.

The stall-optimal solution is a swooping trajectory resembling those observed in experienced birds in both its overall shape (Fig. 3B) and the precise location of its transition point (Fig. 4). The model closely predicted the shape of the observed climb trajectories, but produced a more concave dive trajectory than those we observed (Fig. 3). This discrepancy reflects the model's simplifying assumption of constant lift, which means that turning occurs throughout each phase of the flight (see Methods). Nevertheless, at every combination of bird and perch spacing, over half the observed transition points lay within 6% of the optimum predicted to minimise stall distance, where the total deviation is normalised by perch spacing. In fact, the longitudinal position of the observed transition points did not differ significantly from the predicted optima in a generalized linear mixed effects model fitting the combination

of bird and perch spacing as a random effect (mean longitudinal deviation: -0.9%; 95% CI: -2.6%, 0.8%). The vertical position of the observed transition points was biased upwards slightly (mean vertical deviation: 0.5%; 95% CI: 0.0%, 1.0%) but the variation in both axes was comparable between (longitudinal SD: 3.5%; vertical SD: 1.0%) and within (longitudinal SD: 3.3%; vertical SD: 1.0%) groups. Given the simplicity of the model and the variety of the dynamics it produces (Fig. 3), its close quantitative fit to the data over a range of different perch spacings (Fig. 4) strongly supports our hypothesis that the hawks learned trajectories minimising the distance flown under hazardous post-stall conditions.

How might this work from a control perspective? Feedforward control of our two-phase model of perching amounts to learning the appropriate parameter settings $\{\gamma_0, L_{\mathrm{dive}}, L_{\mathrm{climb}}\}$ for a given perch spacing at a given power input P_{dive}. In principle, the corresponding transition point $\{x_{\mathrm{T}}, y_{\mathrm{T}}, V_{\mathrm{T}}\}$ could serve as a virtual target for closed-loop control of the dive phase, which is the approach taken in one recent implementation of autonomous perching[18]. In practice, we think it more likely that the birds learned to command and regulate their parameter settings directly to produce the nominal swooping trajectory. Having jumped at an initial dive angle γ_0, the lift settings L_{dive} and L_{climb} could be regulated using force feedback from the muscle Golgi tendon organs[38] to command wing or tail pitch. The power setting P_{dive} might also be regulated using strain rate feedback from the muscle spindle cells[38] to command motor unit recruitment. Proprioceptive feedback could further be used to detect incipient stall, perhaps supplemented by sensing of feather deflection under flow reversal[9,10]. This mechanosensory information would have to be combined with optic flow expansion[2,14,39] or static visual cues[6] to enable estimation and minimisation of the gap remaining to be closed under hazardous post-stall conditions. Visual cues will also be important in modifying the nominal trajectory to account for the effects of wind[8]. Vision combined with proprioceptive feedback may therefore be key to the learning and control of the entire perching manoeuvre.

Because the aerodynamic forces that perturb flight can be sensed before any measurable disturbance to the kinematic state of the system has had time to evolve, force feedback has a lower latency than state feedback[40,41]. This is a key attraction of fly-by-feel concepts in experimental autonomous vehicles[42], which have demonstrated some notable successes in gust rejection[43,44]. Our modelling hints at an unexpected role for force feedback in perching, analogous to the role of accelerometer feedback in coordinating turns in high-performance aircraft[45]. It also demonstrates that the usual currencies of time and energy that are optimised in steady flight behaviours[1] are not necessarily minimised in the unsteady manoeuvres of large birds, contrary to findings from smaller birds[2]. Instead, our hawks learned swooping trajectories that minimised the distance flown under hazardous post-stall conditions, reflecting the elevated risks of landing at large size. These findings have implications for deep reinforcement learning in autonomous systems, where identifying an appropriate cost function is key[18]. Maintaining control authority is critical during any unsteady manoeuvre subject to disturbances, so although stall may be necessary to braking just before impact[12,15,18,20-24], penalizing stall in relation to distance to target may be important to acquiring robust manoeuvring capability on-the-fly. Putting this together, we envisage a new generation of autonomous vehicles that combines fly-by-feel with deep reinforcement learning to achieve action intelligence approaching that of birds.

References:

1 Hedenstrom, A. & Alerstam, T. Optimal flight speed of birds. *Philosophical Transactions of the Royal Society of London Series B-Biological Sciences* **348**, 471-487, doi:10.1098/rstb.1995.0082 (1995).

2 Chin, D. D. & Lentink, D. How birds direct impulse to minimize the energetic cost of foraging flight. *Science Advances* **3**, doi:10.1126/sciadv.1603041 (2017).

3 Mills, R., Hildenbrandt, H., Taylor, G. K. & Hemelrijk, C. K. Physics-based simulations of aerial attacks by peregrine falcons reveal that stooping at high speed maximizes catch success against agile prey. *PLoS Comput Biol* **14**, e1006044, doi:10.1371/journal.pcbi.1006044 (2018).

4 Green, P. R. & Cheng, P. Variation in kinematics and dynamics of the landing flights of pigeons on a novel perch. *Journal of Experimental Biology* **201**, 3309-3316 (1998).

5 Berg, A. M. & Biewener, A. A. Wing and body kinematics of takeoff and landing flight in the pigeon (Columba livia). *J Exp Biol* **213**, 1651-1658, doi:10.1242/jeb.038109 (2010).

6 Kress, D., van Bokhorst, E. & Lentink, D. How Lovebirds Maneuver Rapidly Using Super-Fast Head Saccades and Image Feature Stabilization. *PLoS One* **10**, e0129287, doi:10.1371/journal.pone.0129287 (2015).

7 Polet, D. T. & Rival, D. E. Rapid area change in pitch-up manoeuvres of small perching birds. *Bioinspir Biomim* **10**, 066004, doi:10.1088/1748-3190/10/6/066004 (2015).

8 Quinn, D. *et al.* How lovebirds maneuver through lateral gusts with minimal visual information. *Proc Natl Acad Sci U S A* **116**, 15033-15041, doi:10.1073/pnas.1903422116 (2019).

9 Carruthers, A. C., Thomas, A. L. R. & Taylor, G. K. Automatic aeroelastic devices in the wings of a steppe eagle *Aquila nipalensis*. *J Exp Biol* **210**, 4136-4149, doi:10.1242/jeb.011197 (2007).

10 Carruthers, A. C., Thomas, A. L. R., Walker, S. M. & Taylor, G. K. Mechanics and aerodynamics of perching manoeuvres in a large bird of prey. *Aeronautical Journal* **114**, 673-680, doi:10.1017/s0001924000004152 (2010).

11 Pennycuick, C. J. Mechanics of bird migration. *Ibis* **111**, 525-+, doi:10.1111/j.1474-919X.1969.tb02566.x (1969).

12 Wickenheiser, A. M. & Garcia, E. Optimization of Perching Maneuvers Through Vehicle Morphing. *Journal of Guidance, Control, and Dynamics* **31**, 815-823, doi:10.2514/1.33819 (2008).

13 Maynard Smith, J. The importance of the nervous system in the evolution of animal flight. *Evolution* **6**, 127-129, doi:10.2307/2405510 (1952).

14 Lee, D. N., Davies, M. N. O., Green, P. R. & Van der Weel, F. R. R. Visual control of velocity of approach by pigeons when landing. *Journal of Experimental Biology* **180**, 85-104 (1993).

15 Moore, J., Cory, R. & Tedrake, R. Robust post-stall perching with a simple fixed-wing glider using LQR-Trees. *Bioinspir Biomim* **9**, 025013, doi:10.1088/1748-3182/9/2/025013 (2014).

16 Zhang, Z., Xie, P. & Ma, O. Bio-Inspired Trajectory Generation for UAV Perching Movement Based on Tau Theory. *International Journal of Advanced Robotic Systems* **11**, doi:10.5772/58898 (2014).

17 Chirarattananon, P., Ma, K. Y. & Wood, R. J. Perching with a robotic insect using adaptive tracking control and iterative learning control. *The International Journal of Robotics Research* **35**, 1185-1206, doi:10.1177/0278364916632896 (2016).

18 Waldock, A., Greatwood, C., Salama, F. & Richardson, T. Learning to Perform a Perched Landing on the Ground Using Deep Reinforcement Learning. *Journal of Intelligent & Robotic Systems* **92**, 685-704, doi:10.1007/s10846-017-0696-1 (2017).

19 Novati, G., Mahadevan, L. & Koumoutsakos, P. Controlled gliding and perching through deep-reinforcement-learning. *Physical Review Fluids* **4**, doi:10.1103/PhysRevFluids.4.093902 (2019).

20 Cory, R. & Tedrake, R. in *AIAA Guidance, Navigation & Control Exhibit* (American Institute of Aeronautics and Astronautics, Honolulu, Hawaii, 2008).

21 Lussier Desbiens, A., Asbeck, A. T. & Cutkosky, M. R. Landing, perching and taking off from vertical surfaces. *The International Journal of Robotics Research* **30**, 355-370, doi:10.1177/0278364910393286 (2011).

22 Paranjape, A. A., Chung, S.-J. & Kim, J. Novel Dihedral-Based Control of Flapping-Wing Aircraft With Application to Perching. *IEEE Transactions on Robotics* **29**, 1071-1084, doi:10.1109/tro.2013.2268947 (2013).

23 Greatwood, C., Waldock, A. & Richardson, T. Perched landing manoeuvres with a variable sweep wing UAV. *Aerospace Science and Technology* **71**, 510-520, doi:10.1016/j.ast.2017.09.034 (2017).

24 Roderick, W. R., Cutkosky, M. R. & Lentink, D. Touchdown to take-off: at the interface of flight and surface locomotion. *Interface Focus* **7**, 20160094, doi:10.1098/rsfs.2016.0094 (2017).

25 Provini, P., Tobalske, B. W., Crandell, K. E. & Abourachid, A. Transition from wing to leg forces during landing in birds. *J Exp Biol* **217**, 2659-2666, doi:10.1242/jeb.104588 (2014).

26 Crandell, K. E., Smith, A. F., Crino, O. L. & Tobalske, B. W. Coping with compliance during take-off and landing in the diamond dove (Geopelia cuneata). *PLoS One* **13**, e0199662, doi:10.1371/journal.pone.0199662 (2018).

27 Roderick, W. R., Chin, D. D., Cutkosky, M. R. & Lentink, D. Birds land reliably on complex surfaces by adapting their foot-surface interactions upon contact. *Elife* **8**, doi:10.7554/eLife.46415 (2019).

28 Tang, D. *et al.* Shape reconstructions and morphing kinematics of an eagle during perching manoeuvres. *Chinese Physics B* **29**, doi:10.1088/1674-1056/ab610a (2020).

29 Polet, Delyle T., Rival, David E. & Weymouth, Gabriel D. Unsteady dynamics of rapid perching manoeuvres. *Journal of Fluid Mechanics* **767**, 323-341, doi:10.1017/jfm.2015.61 (2015).

30 Song, J. Fly low: The ground effect of a barn owl (Tyto alba) in gliding flight. *Proceedings of the Institution of Mechanical Engineers, Part C: Journal of Mechanical Engineering Science* **235**, 308-318, doi:10.1177/0954406220943939 (2020).

31 Wang, Y., Tobalske, B. W., Cheng, B. & Deng, X. Gravitation-enabled Forward Acceleration during Flap-bounding Flight in Birds. *Journal of Bionic Engineering* **15**, 505-515, doi:10.1007/s42235-018-0041-9 (2018).

32 Goldstein, H., Poole, C. & Safko, J. *Classical Mechanics*. 3rd edn, (Addison Wesley, 2002).

33 Tucker, V. A. & Heine, C. Aerodynamic of gliding flight in a Harris' Hawk, *Parabuteo unicintus*. *Journal of Experimental Biology* **149**, 469-489 (1990).

34 Pennycuick, C. J., Fuller, M. R. & McAllister, L. Climbing performance of Harris' Hawks (*Parabuteo unicinctus*) with added load – implications for muscle mechanics and for radiotracking. *Journal of Experimental Biology* **142**, 17-29 (1989).

35 Van Walsum, T. A. *et al.* Exploring the relationship between flapping behaviour and accelerometer signal during ascending flight, and a new approach to calibration. *Ibis* **162**, 13-26, doi:10.1111/ibi.12710 (2019).

36 Reich, G. W., Eastep, F. E., Altman, A. & Albertani, R. Transient Poststall Aerodynamic Modeling for Extreme Maneuvers in Micro Air Vehicles. *Journal of Aircraft* **48**, 403-411, doi:10.2514/1.C000278 (2011).

37 Uhlig, D. V. & Selig, M. S. Modeling Micro Air Vehicle Aerodynamics in Unsteady High Angle-of-Attack Flight. *Journal of Aircraft* **54**, 1064-1075, doi:10.2514/1.C033755 (2017).

38 Granatosky, M. C. *et al.* Variation in limb loading magnitude and timing in tetrapods. *J Exp Biol* **223**, doi:10.1242/jeb.201525 (2020).

39 Davies, M. N. O. & Green, P. R. Optic flow-field variables trigger landing in hawk but not in pigeons. *Naturwissenschaften* **77**, 142-144, doi:10.1007/bf01134481 (1990).

40 Thompson, R. A., Evers, J. H. & Stewart, K. C. in *AIAA Atmospheric Flight Mechanics Conference* (American Institute of Aeronautics and Astronautics, Toronto, Ontario, Canada, 2010).

41 Gremillion, G. M., Castano, L. & Humbert, J. S. in *AIAA Guidance, Navigation, and Control Conference* (American Institute of Aeronautics and Astronautics, Kissimmee, FL, 2015).

42 Yeo, D., Atkins, E. M., Bernal, L. P. & Shyy, W. Fixed-Wing Unmanned Aircraft In-Flight Pitch and Yaw Control Moment Sensing. *Journal of Aircraft* **52**, 403-420, doi:10.2514/1.C032682 (2015).

43 Araujo-Estrada, S. A. *et al.* in *AIAA Guidance, Navigation, and Control Conference* (2017).

44 Castano, L., Airoldi, S., McKenna, T. & Humbert, J. S. in *14th AIAA Aviation Technology, Integration, and Operations Conference* (American Institute of Aeronautics and Astronautics, Atlanta, GA, 2014).

45 Stevens, B. L. & Lewis, F. L. *Aircraft Control and Simulation*. (John Wiley & Sons Inc., 2003).

46 Potier, S., Mitkus, M. & Kelber, A. High resolution of colour vision, but low contrast sensitivity in a diurnal raptor. *Proc Biol Sci* **285**, doi:10.1098/rspb.2018.1036 (2018).

Table 1. Measurements and model parameters by bird.

	sex	age	m (kg)	b (m)	S (m^2)	$\bar{V}_0$ (m s^{-1})	$\bar{V}_{\mathrm{end}}$ (m s^{-1})	$\hat{P}_{\mathrm{dive}}/m$ (W kg^{-1})
Drogon	♂	juv.	0.660	1.01	0.1895	3.9	2.3	22.86
Rhaegal	♂	juv.	0.620	1.02	0.1918	4.0	2.5	18.73
Ruby	♀	ad.	0.874	1.08	0.2146	3.9	2.3	22.50
Toothless	♂	juv.	0.738	1.07	0.2098	3.8	2.5	22.74

juv. juvenile; ad. adult; m total mass; b wingspan; S wing area; $\bar{V}_0$ mean observed take-off speed; $\bar{V}_{\mathrm{end}}$ mean observed landing speed; $\hat{P}_{\mathrm{dive}}/m$ specific power setting estimate.

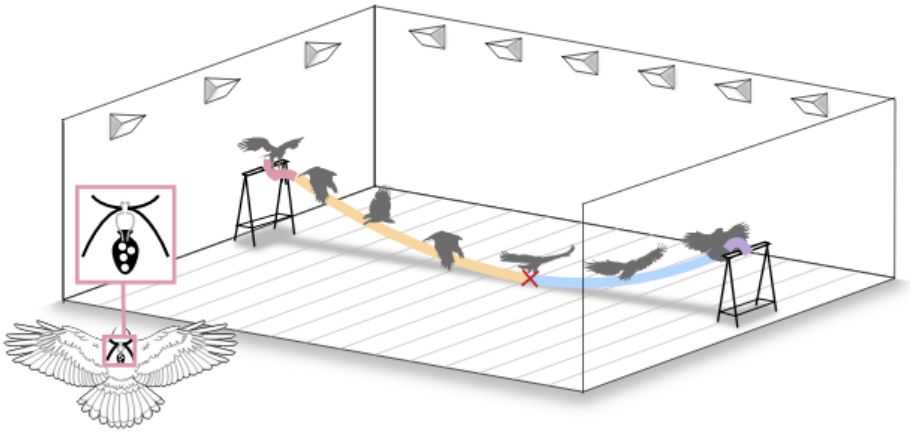

Figure 1. Schematic of characteristic swooping trajectory and data acquisition. Harris' hawks were flown between perches in a purpose-built motion capture studio, whilst wearing a template of retroreflective markers close to the centre of mass (inset panel). Swooping was initiated by a take-off jump (red line) followed by a powered dive (yellow line) transitioning at its lowest point (red cross) into an unpowered climb (blue line) involving a rapid pitch-up manoeuvre and ending with the body almost vertical and the wings outstretched as the feet contacted the landing perch (purple line).

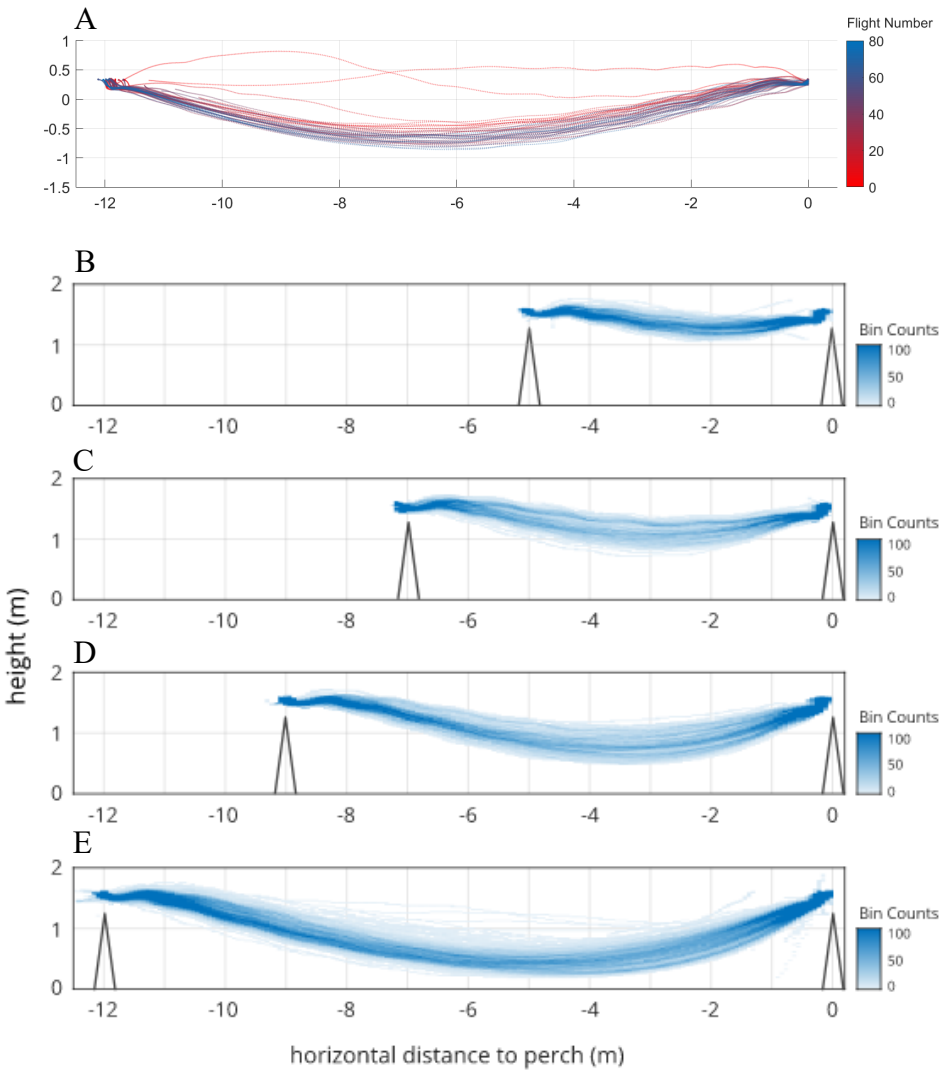

Figure 2. Measured swooping trajectories for all flights. (A) Ontogeny of the $N = 45$ complete flight trajectories recorded at 12 m perch spacing for juvenile bird "Toothless": note the more direct trajectory taken on the earlier flights, and quick acquisition of the swooping trajectory characteristic of experienced birds; some trajectories missing due to data dropout. (**B-E**) Spatial histograms showing pooled trajectory data from all $N = 1{,}592$ flights and all $n = 4$ hawks at (B) 5 m, (C) 7 m, (D) 9 m, and (E) 12 m perch spacing; note the consistency of the swooping trajectories observed under each test condition.

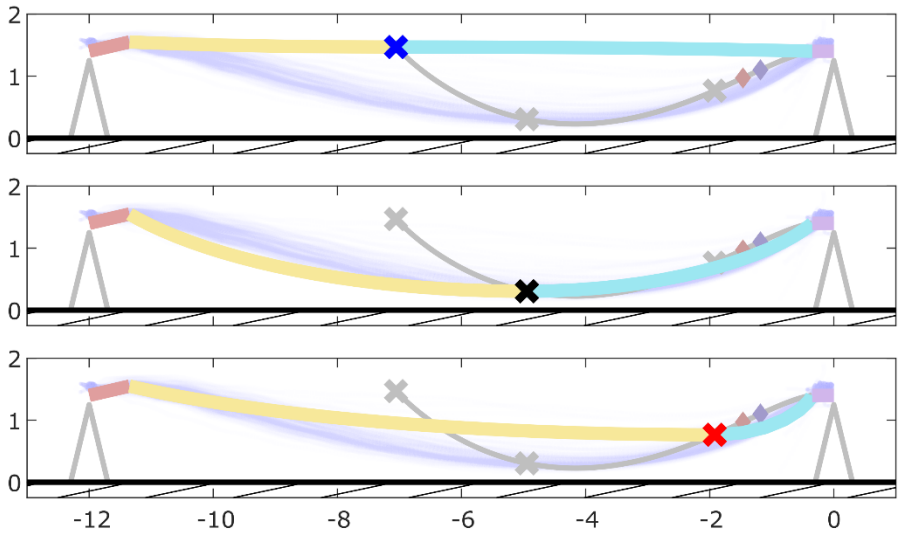

Figure 3. Optimal perching trajectories minimising different cost functions. Solid lines show trajectories predicted for bird "Drogon" at 12 m perch spacing under the two-phase model of perching, comprising a powered dive at the best-fitting power setting of 22.9 W kg^{-1} (yellow line), transitioning into an unpowered climb (blue line) and minimising: **(A)** energetic cost (blue cross); **(B)** stall distance (black cross); or **(C)** flight duration (red cross). The optimal transition point (crosses) along the line of feasible transition points (grey line) is only close to the observed transition point at the bottom of the flight trajectory if stall distance is optimised (B); observed trajectories are shown as a spatial histogram (lilac shading).

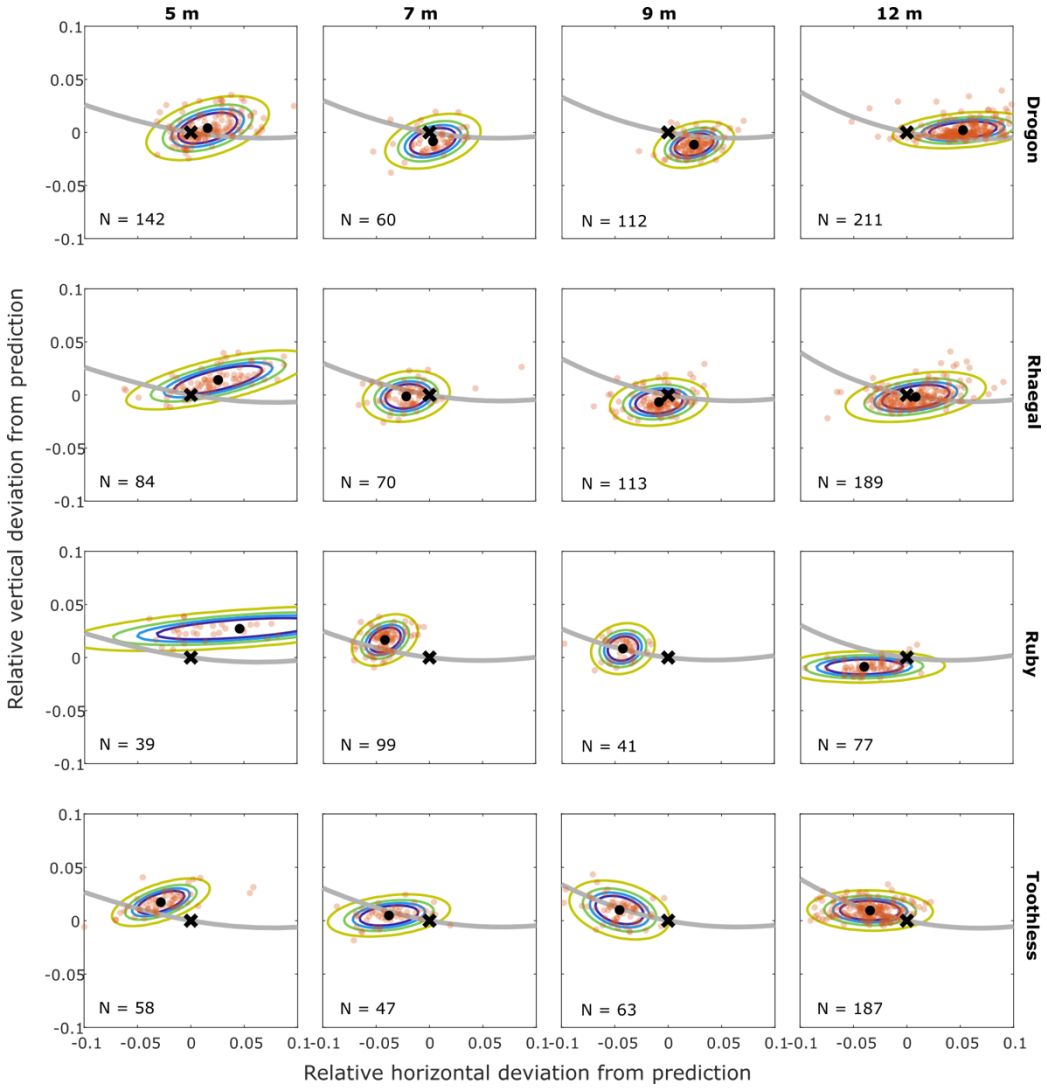

Figure 4. Fit of observed transition points to optima minimising stall distance. At each combination of bird and perch spacing, the *N* observed transition points (red dots) are compared to the optimal transition point predicted to minimise stall distance under the model (black cross). Black dot denotes the sample mean for each test condition; coloured contours denote the 50th to 95th percentiles of a bivariate normal distribution fitted to the data, at 5% intervals; grey line denotes the line of feasible transition points predicted under the model. Distance deviation is shown as a proportion of perch spacing distance.

METHODS

Experimental setup. We flew $n = 4$ captive-bred Harris' Hawks (*Parabuteo unicinctus*) between two 1.25 m high A-frame perches positioned 5, 7, 9, or 12 m apart in a purpose-built motion capture studio (Fig. 1; Supplementary Movie 1). The sample comprised 3 inexperienced juvenile males (approximately 4-6 months old), and an experienced adult female (7 years old); see Table 1. The flights were undertaken in a windowless hall measuring 20.2 m x 6.1m, with a minimum ceiling height of 3.8m and walls hung with camouflage netting to provide visual contrast. Flicker-free LED lights provided a mixture of direct 4000 K lighting and indirect 5000 K lighting at approximately 1000 lux, designed to mimic overcast morning or evening light.

Experimental design. Data were collected over 11 weeks of flight testing, with each bird flying freely between the perches on a variable number of flights up to approximately 30 per session. The bird was motivated to fly from its take-off perch by the presentation of a small food reward on the landing perch. The birds usually responded immediately to the presentation of the food reward, and the session was ended if the bird appeared visibly tired or lacking in motivation. The birds received a larger food reward at the end of the session. Perch spacing was set at 8 m during an initial fitness-training period, which we did not include in the main analysis. Perch spacing was maintained at 12 m for the first 3 weeks of experiments, before being pseudo-randomised at 5, 7 or 9 m perch spacing on every day thereafter.

Ethics statement. This work was approved by the Animal Welfare and Ethical Review Board of the Department of Zoology, University of Oxford, in accordance with University policy on the use of protected animals for scientific research, permit no. APA/1/5/ZOO/NASPA, and is considered not to pose any significant risk of causing pain, suffering, damage or lasting harm to the animals.

Motion capture. We reconstructed the birds' flight trajectories using a 20-camera motion capture system (Vantage 16, Vicon Motion Systems Ltd, Oxford, UK) mounted 3 m above the

floor on scaffolding fixed around the walls. The motion capture system was turned on at least one hour before the start of the experiments, and was calibrated shortly before the first session (Active Calibration Wand, Vicon Motion Systems Ltd, Oxford, UK), using Vicon Nexus software for data acquisition and reconstruction. The motion capture cameras were set to record at 120 or 200 Hz under stroboscopic 850 nm infrared illumination, well outside the visible spectrum of these birds[46], and a set of four high-definition video cameras (Vue, Vicon Motion Systems Ltd, Oxford, UK) recorded synchronised reference video at 120 or 100 Hz, respectively. Each hawk was fitted with a rigid marker template comprising four 6.4mm diameter spherical retroreflective markers (Fig. 1) worn on a backpack secured by a pair of Teflon ribbons (TrackPack Mounting System, Marshall Radio Telemetry, UT, USA). The birds sometimes wore other retroreflective markers carried on the head, wings, or tail, but these are not included in the present analysis. A pair of 9.5 mm diameter spherical retroreflective markers was fixed to either end of each perch.

Marker reconstruction. We used Vicon Nexus software to reconstruct the positions of the markers within the flight volume, using a coordinate system corresponding to the principal axes of the flight hall. We removed any flights for which there were long sections of missing data, or for which the bird did not land at the perch, resulting in a sample of $n = 1592$ flight trajectories suitable for analysis. This comprised $n = 664$ flights recorded at 12 m perch spacing, $n = 329$ flights at 9 m spacing, $n = 276$ flights at 7 m spacing, and $n = 323$ flights at 5 m spacing. The backpack and tail mount markers were usually visible on >70% of the recorded frames, but because of a challenging combination of dense marker placement, intermittent marker occlusion, and high-speed motion, the proprietary marker tracking algorithms were not uniformly successful in matching markers between frames. In addition, patches of specular reflection from the worn equipment sometimes appeared as ghost markers. Consequently, although the Nexus software reconstructed the positions of all visible markers

to a high degree of accuracy, it was not always able to label each marker reliably, or to identify every marker on every frame. We therefore wrote a custom script in MATLAB v2018a (Mathworks, MA, USA) which analysed the pattern of pairwise distances between markers in the rigid templates to label the anonymous markers (see Supporting Code).

Marker labelling. The anonymous markers were labelled separately for each frame by using Procrustes analysis to match any visible markers to the known backpack template. We used the centroid of the resulting set of candidate backpack markers as an initial estimate of backpack position and fitted a quintic spline to interpolate its position on frames with missing data. We then used our initial or interpolated estimate of the backpack's position on each frame to define a search volume matched to the size of the backpack template and labelled any other markers falling within this search volume as candidate backpack markers. This two-stage labelling approach was able to accommodate missing markers and occasional ghost markers, and successfully identified the correct number of markers in >80% of all frames in which the backpack markers were visible. As the backpack sat directly between the scapulars, we took the centroid of the candidate backpack markers to approximate the position of the bird's centre of mass, and estimated its velocity and acceleration by fitting and differentiating the smoothest quintic spline function passing through the positions measured on each frame.

Trajectory analysis. Because the take-off and landing perches were located at the same height, every flight necessarily involved a powered flapping phase to replace the drag losses. The three juvenile males flew directly between the perches on their first flights, but quickly adopted the deep swooping trajectory typical of experienced birds including the adult female. This behaviour, which is characteristic of most large birds when perching, involves a powered dive followed by an unpowered climb. Because the birds morphed smoothly between flapping and gliding flight, it was not possible to identify a unique point at which this transition occurred with reference to the wing kinematics. We instead identified the transition as occurring at the

lowest point in the bird's flight trajectory, which coincides with the end of the powered phase and represents the point in the trajectory when the bird has borrowed the most energy from its environment. We estimated the location of this point by using the 30-point moving mean of the measured backpack position to smooth out any vertical oscillations due to flapping.

Take-off and landing. Each flight was initiated by a jump during which the feet remained in contact with the perch (Supplementary Movie 1). This jump phase ended with a jerk as the feet released from the perch, but the noise associated with the measured acceleration, particularly during flapping, makes it an unreliable marker of the onset of the flight phase. We therefore defined the flight proper as beginning when the backpack reached a horizontal distance of 0.65 m from the take-off perch axis, this threshold distance being determined through visual inspection of the angular acceleration traces over many flights. The point of contact with the landing perch was likewise associated with a pronounced linear and angular acceleration, but for similar reasons we define the flight proper as ending when the backpack reached a horizontal distance of 0.35 m from the landing perch axis. The difference in these two threshold distances relates to the fact that the bird's legs were fully extended at take-off and partially flexed upon landing. In each case, we found that the backpack was located approximately 0.15 m above the perch.

Flight mechanics model. To identify what flight performance objective(s) were optimised by the birds' characteristic swooping trajectory, we built a simplified flight mechanics model of each bird for each of the two flight phases (see Supporting Code). As a first-order modelling approach, we assumed constant aerodynamic lift (L) and power (P) on each phase, using settings $L = L_{\mathrm{dive}}$ and $P = P_{\mathrm{dive}}$ for the powered dive phase, and $L = L_{\mathrm{dive}}$ and $P = 0$ for the unpowered climb phase, where lift L is defined as the component of the aerodynamic force perpendicular to the flight path. Aerodynamic thrust (T) acting tangent to the flight path is modelled as $T = P/V$ during the powered phase, where V is the bird's airspeed neglecting any

induced velocity component. This is opposed by aerodynamic drag (D), which we model as the sum of a lift-induced drag component and a combined parasite and profile drag component:

$$D = kL\left(-\frac{1}{2} + \sqrt{\frac{1}{4} + \left(\frac{2L}{\rho\pi b^2 V^2}\right)^2}\right)^{\frac{1}{2}} + \frac{1}{2}\rho V^2 S C_D \tag{1}$$

where $\rho = 1.23$ kg m^{-3} is air density, b is wingspan, and where S is wing area which we assumed to be maximal throughout the manoeuvre (Table 1). The dimensionless induced drag factor $k = 1.623$ and combined profile and parasite drag coefficient $C_D = 0.00994$ were estimated empirically from a published glide polar measured for a Harris' hawk[33]. This was done by regressing the measured drag against the predictors on the righthand side of Eq. 1. The rate of change in airspeed and flight path elevation angle (γ) can therefore be expressed as:

$$\dot{V} = \frac{1}{m}\left(\frac{P}{V} - D(L,V)\right) - g\sin\gamma$$

$$\dot{\gamma} = \frac{1}{V}\left(\frac{L}{m} - g\cos\gamma\right) \tag{2a,b}$$

where g is gravitational acceleration and m is the bird's mass.

We modelled the resulting flight trajectories in lab-fixed Cartesian coordinates (x,y) by coupling Eqs. 1-2 for $\dot{V}$ and $\dot{\gamma}$ with the component kinematics equations:

$$\dot{x} = V_x$$

$$\dot{y} = V_y$$

$$\dot{V}_x = \frac{\dot{V}}{V}V_x - \dot{\gamma}V_y$$

$$\dot{V}_y = \frac{\dot{V}}{V}V_y + \dot{\gamma}V_x \tag{3a-d}$$

with $V = \sqrt{V_x^2 + V_y^2}$. We integrated these ordinary differential equations numerically using the ode45 solver in MATLAB, which is based on an explicit Runge-Kutta (4,5) formula, the Dormand-Price pair.

Trajectory simulations. We simulated each bird individually to account for variation in flight morphology. We matched the initial speed $V(0)$ of the simulations to the mean take-off speed $\bar{V}_0$ observed for each bird at the threshold horizontal distance of 0.65 m from the take-off perch (Table 1). We treated the initial dive angle $\gamma(0)$ as a free parameter γ_0, so the initial conditions for integrating Eqs. 3a-d were $V_x(0) = \bar{V}_0 \cos\gamma_0$ and $V_y = \bar{V}_0 \sin\gamma_0$ with $x(0) = 0.65$ m and $y(0) = 1.35$ m. We modelled the powered dive phase by assuming a fixed constant power setting $P = P_{\mathrm{dive}}$ in Eq. 2a, and by treating the constant lift setting in Eqs. 1-2a,b as a free parameter $L = L_{\mathrm{dive}}$. We optimised P_{dive} separately for each bird (see Main Text). With these assumptions, and for a given constant power setting P_{dive}, each pair of free parameter settings $\{\gamma_0, L_{\mathrm{dive}}\}$ defines a unique flight trajectory for the powered flight phase. A subset of these powered dive trajectories passes through the horizontal, in the sense of having a turning point $(x_{\mathrm{T}}, y_{\mathrm{T}})$ at which $V_y = 0$ with $V_x \neq 0$. This subset defines the set of reachable combinations of position and speed at which the transition from powered to unpowered flight can occur under the model.

The initial conditions for the unpowered climb phase are given by the position $(x_{\mathrm{T}}, y_{\mathrm{T}})$ and velocity $(V_{\mathrm{T}}, 0)$ of the bird at this transition point. Each pair of parameter settings $\{\gamma_0, L_{\mathrm{dive}}\}$ for the powered dive phase therefore defines a family of possible flight trajectories for the unpowered climb phase, parameterised only by its constant lift setting $L = L_{\mathrm{climb}}$. Hence, for any given pair of parameter settings $\{\gamma_0, L_{\mathrm{dive}}\}$, we are left only to solve for the unique value of L_{climb} that will produce a trajectory intercepting the point of contact with the landing perch at $x = s - 0.35$ m and $y = 1.35$ m, where s is the perch spacing (see above). In practice, there are only certain combinations of $\{\gamma_0, L_{\mathrm{dive}}\}$ that will bring the simulated bird to

the landing perch at a realistic speed, so it proved most efficient computationally to solve the unpowered climb phase backwards in time from the point of contact with the landing perch, and to match solutions for the two flight phases at the transition point (see Code S1). We therefore fixed the initial speed of this backwards simulation of the unpowered climb phase to the mean landing speed $\bar{V}_{\mathrm{end}}$ observed for each at the threshold horizontal distance of 0.35 m from the landing perch (Table 1). For the purposes of finding matching solutions, we treated both the flight path angle at the point of contact (γ_{end}) and the constant lift setting for the unpowered flight phase (L_{climb}) as free parameters. These then free parameters $\{\gamma_{\mathrm{end}}, L_{\mathrm{climb}}\}$ become fixed for a given pair of parameter settings $\{\gamma_0, L_{\mathrm{dive}}\}$ once the matching solution for the powered flight phase is found.

Feasible trajectory search. We identify feasible trajectories as those which bring an individual bird to its landing perch at the same mean speed and position as we observed in the experiments. For a given constant power setting P_{dive}, this constraint defines a line of feasible transition points corresponding to a line of feasible parameter settings $\{\gamma_0, L_{\mathrm{dive}}\}$. We implemented the search for feasible transition points as a constrained minimisation problem solved using an interior-point algorithm in MATLAB. We constrained the difference in transition point position $(x_{\mathrm{T}}, y_{\mathrm{T}})$ and velocity $(V_{\mathrm{T}}, 0)$ between the end of the powered phase and start of the unpowered phase to be zero. We then solved for the parameter settings $\{\gamma_0, L_{\mathrm{dive}}\}$ and $\{\gamma_{\mathrm{end}}, L_{\mathrm{climb}}\}$ that would have placed the transition point exactly at the landing perch. We took these parameter settings as initial values when solving for the parameter settings that would have caused the transition point to be placed a small increment ahead of the perch, which we set as the target of the minimisation. We repeated this process to place the transition point another small increment in distance ahead of the perch, inheriting the parameter settings of the previous solution as initial values for the next round, until the complete line of feasible transition points had been found. It is important to note that other transition points falling close to this line could

also be physically feasible in the sense of bringing the bird to the landing perch, but will be associated with higher or lower speeds at the point of contact.

Trajectory optimisation. The unique mapping that exists between parameter settings $\{\gamma_0, L_{\mathrm{dive}}\}$ and transition point $\{x_{\mathrm{T}}, y_{\mathrm{T}}, V_{\mathrm{T}}\}$ means that any property of a given flight trajectory is also a property of its transition point. This includes the duration (τ) and energetic cost (E) of the flight, and the distance from the landing perch at which deep stall occurs (d_{stall}) – each of which may be considered candidate optimisation targets. We identified the optimal transition point at which each of these targets was minimised by a direct search along the line of feasible transition points. Under the two-phase model of perching, the duration of a flight trajectory is implicit in its solution as $\tau = \tau_{\mathrm{dive}} + \tau_{\mathrm{climb}}$. Minimising the total flight duration τ therefore entails jointly minimising the duration of the powered dive phase τ_{dive} and the unpowered phase τ_{climb}. In contrast, given the constant power assumption, the energetic cost of a flight trajectory is simply $E = P_{\mathrm{dive}}\tau_{\mathrm{dive}}$, so for a given constant power setting P_{dive}, minimising the energetic cost of the flight is equivalent to minimising the duration of the powered phase τ_{dive} alone. Wing stall is a complex phenomenon, so we did not model its effects directly. However, because lift varies as $L = \rho V^2 S C_L/2$, stall is implicit in the very high values of the lift coefficient C_L that are necessary to meet the constant lift requirement $L = L_{\mathrm{glide}}$ at the low speeds V reached as the bird decelerates on approach to the perch. Minimising the distance flown post-stall therefore amounts to penalising flight at values of C_L exceeding some specified threshold (see Main Text).

Author contributions: MKH, **LAF** Conceptualization, Methodology, Software, Formal analysis, Investigation, Writing – original draft, Writing – review & editing, Visualization. **GT** Conceptualization, Methodology, Investigation, Resources, Writing – original draft, Writing – review & editing, Supervision, Project administration, Funding acquisition.

Competing interests: The authors declare no competing interests.

Additional information: Supplementary Information is available for this paper. Correspondence and requests for materials should be addressed to graham.taylor@zoo.ox.ac.uk.

Data and code availability: The motion capture data and code that support the findings of this study are available in figshare with the identifier doi:10.6084/m9.figshare.16529328

.